The Company of **Biologists**

RESEARCH REPORT

Primordial germ cells adjust their protrusion type while migrating in different tissue contexts *in vivo*

Lukasz Truszkowski[1], Dilek Batur[1], Hongyan Long[2], Katsiaryna Tarbashevich[1], Bart E. Vos[3], Britta Trappmann[2] and Erez Raz[1,4,*]

ABSTRACT

In both physiological processes and disease contexts, migrating cells have the ability to adapt to conditions in their environment. As an *in vivo* model for this process, we use zebrafish primordial germ cells that migrate throughout the developing embryo. When migrating within an ectodermal environment, the germ cells form fewer and smaller blebs when compared with their behavior within mesodermal environment. We find that cortical tension of neighboring cells is a parameter that affects blebbing frequency. Interestingly, the change in blebbing activity is accompanied by the formation of more actin-rich protrusions. These alterations in cell behavior that correlate with changes in RhoA activity could allow the cells to maintain dynamic motility parameters, such as migration speed and track straightness, in different settings. In addition, we find that the polarity of the cells can be affected by stiff structures positioned in their migration path

This article has an associated 'The people behind the papers' interview.

KEY WORDS: Zebrafish, Migration, Protrusion, Bleb, Germ cell, Amoeboid motility

INTRODUCTION

Primordial germ cells (PGCs) are typically specified away from the region where the gonad develops, such that they must migrate towards a region in the embryo where they associate with cells of mesodermal origin to form the gonad (Barton et al., 2016; Grimaldi and Raz, 2020; Richardson and Lehmann, 2010). During their migration, PGCs encounter multiple types of cells and tissues. This is especially evident in zebrafish, where PGCs are specified at four locations that are randomly oriented relative to the embryonic axis (Weidinger et al., 1999). Starting from the positions where they originate, PGCs migrate through the

[1]Institute of Cell Biology, ZMBE, University of Münster, D-48149 Münster, Germany. [2]Bioactive Materials Laboratory, Max Planck Institute for Molecular Biomedicine, D-48149 Münster, Germany. [3]Third Institute of Physics – Biophysics, Georg August University Göttingen, D-37007 Göttingen, Germany. [4]Max Planck Institute for Molecular Biomedicine, D-48149, Münster, Germany.

*Author for correspondence (erez.raz@uni-muenster.de)

L.T., 0000-0001-7816-6092; D.B., 0000-0002-2585-6150; H.L., 0000-0001-9748-4301; B.E.V., 0000-0002-4325-6298; B.T., 0000-0002-6260-4075; E.R., 0000-0002-6347-3302

embryo as the tissues around them undergo processes of differentiation and morphogenesis. Accordingly, to reach their target, PGCs have to move within tissues that exhibit different biophysical properties.

The migration of zebrafish PGCs is guided by the chemokine Cxcl12a, which binds the receptor Cxcr4b (Doitsidou et al., 2002). Interestingly, in the absence of the guidance cue or its receptor, the PGCs remain motile and migrate non-directionally within the whole embryo (Doitsidou et al., 2002; Gross-Thebing et al., 2020). Zebrafish PGCs perform ameboid motility, which is characterized by extensive cell body deformations, low substrate attachment and generation of actin-based pseudopods or hydrostatic pressure-powered blebs (Paluch and Raz, 2013; Yamada and Sixt, 2019; Charras et al., 2006; Schick and Raz, 2022). A range of studies conducted mainly in *in vitro* settings show that cells can alter their protrusion type or migration mode when located in different 2D and 3D environments (Lämmermann and Germain, 2014; Liu et al., 2015; Talkenberger et al., 2017; te Boekhorst et al., 2016). Here, we use zebrafish PGCs as an accessible *in vivo* model for exploring how amoeboid cells respond to changes in the properties of their environment.

We show that PGCs migrate efficiently in different cellular contexts and respond to differences in biophysical properties of their environment by adjusting the protrusion type they produce. We also highlight the cortex tension of surrounding cells as a parameter influencing the protrusive activity.

RESULTS AND DISCUSSION

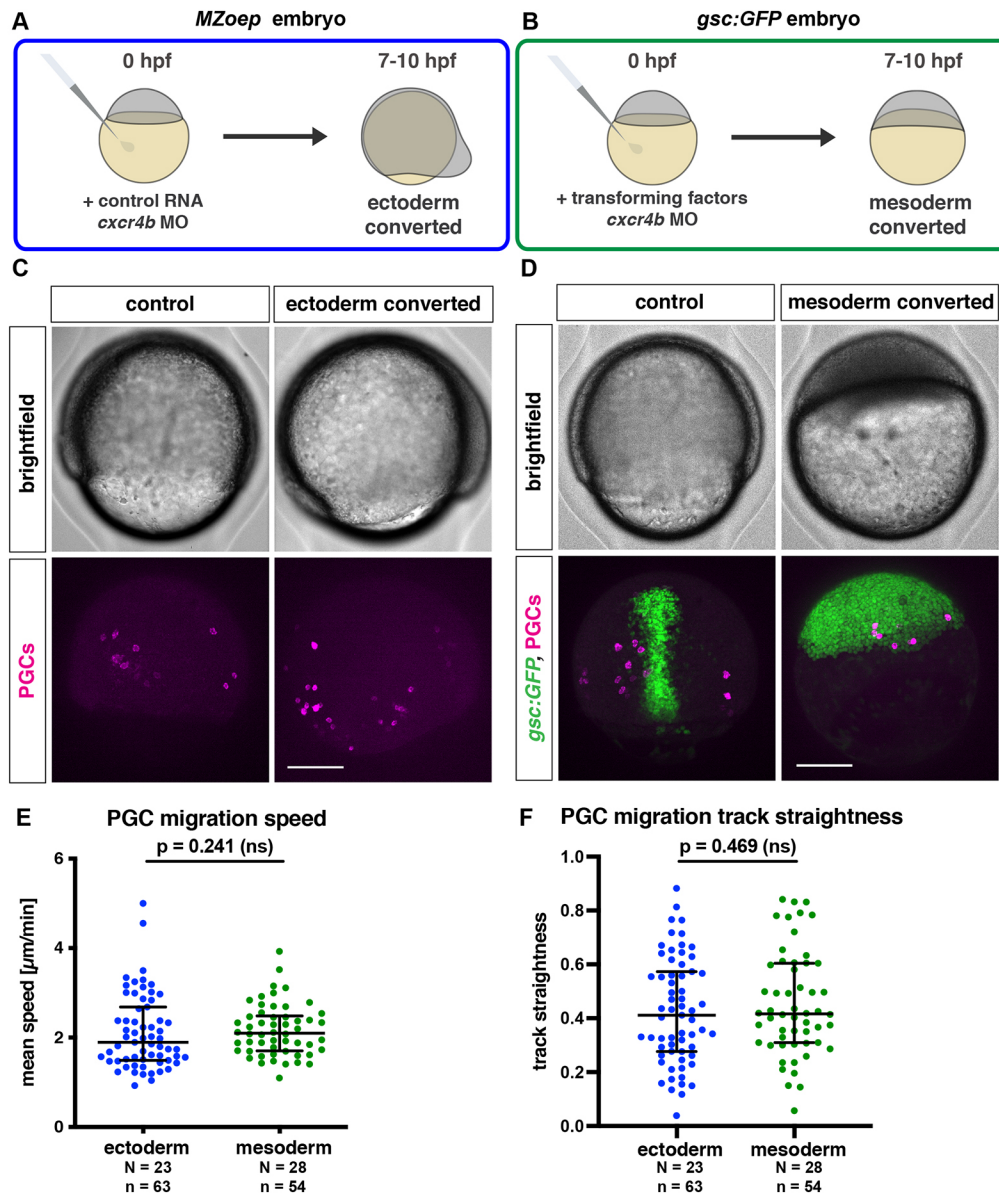### Migration of PGCs within different embryonic germ layers

PGCs lacking the guidance receptor Cxcr4b can be found within ectodermal, mesodermal and endodermal tissues (Fig. S1A; Gross-Thebing et al., 2020). These different germ layers present PGCs with environments that have distinct biophysical properties (Krieg et al., 2008), allowing us to study the behavior of the cells in different tissue contexts within the live animal. To ensure uniform conditions around the Cxcr4b-depleted PGCs, we generated embryos with a single germ layer, according to previously established protocols (Krieg et al., 2008) (Fig. 1A-D, Fig. S1B). Importantly, these experimental conditions do not affect the identity of PGCs, as determined by the expression levels of germ cell-specific RNA markers (Fig. S1C,D), in line with studies demonstrating the robustness of the PGC fate in face of somatic differentiation cues (Gross-Thebing et al., 2017; Strome and Updike, 2015).

As a first step in characterizing the dynamic behavior of PGCs located within different germ layers, we monitored their migration speed and track straightness. Interestingly, we found these parameters to be similar for cells located within the ectoderm and the mesoderm, despite the previously described differences in tissue properties (Fig. 1E,F).

DEVELOPMENT

1

Fig. 1. Migration of PGCs within ectodermal and mesodermal tissues. (A) Schematic depiction of the generation of embryos composed of ectodermal cells. In maternal-zygotic *one eye pinhead* mutant embryos (*MZoep*), all the somatic cells develop into ectoderm, with Cxcr4b expression inhibited by injection of *cxcr4b* morpholino. (B) Conversion of embryonic cells into mesoderm is achieved by co-injection of RNA encoding a Nodal ligand (*cyclops*) and a morpholino directed against the RNA encoding the transcription factor Sox32 (together referred to as 'transforming factors'). (C) Lateral views of control and ectoderm-converted embryos (upper panels), with the PGCs labeled (magenta, lower panels). (D) Dorsal views showing control and mesoderm-converted embryos (upper panels) with the PGCs labeled (magenta) and the expression of GFP driven by the *goosecoid* promoter (green) in the corresponding embryos (lower panels). Scale bars: 200 µm. (E,F) Migration speed (E) and track straightness (F) of PGCs migrating within ectodermal and mesodermal tissues. The graphs show the median; whiskers indicate the interquartile range (IQR). For speed comparison (E), a Mann–Whitney test was performed; for straightness comparison (F), a two-tailed *t*-test was performed. *N* and *n* represent numbers of embryos and cells, respectively.

The effect of the cellular environment on bleb dynamics

Zebrafish PGCs primarily generate bleb-like rapidly inflating round actin-free protrusions that facilitate the movement of the cell (Blaser et al., 2006; Goudarzi et al., 2017; Olguin-Olguin et al., 2021). To determine whether features of the cellular environment influence the protrusive activity, we monitored the frequency of bleb formation and the size of blebs. Interestingly, PGCs migrating within the ectodermal tissue formed fewer and smaller blebs when compared with those formed by cells located within the mesodermal tissue (Fig. 2A-C). These results were further supported by analyzing blebbing in wild-type PGCs transplanted into either ectoderm-converted or control embryos. Here, fewer and smaller blebs were generated by PGCs transplanted into the ectodermal environment when compared with controls (Fig. S2).

As blebs are formed more frequently in cells migrating under confinement (Liu et al., 2015; Ruprecht et al., 2015), we examined the density of the nuclei within converted embryos and found that it did not differ between ectodermal and mesodermal tissues (Fig. S3).

Relative to the other germ layers, ectodermal cells possess higher cortex tension, which is primarily generated by myosin contractility (Krieg et al., 2008). To examine whether this feature affects the behavior of the PGCs, we reduced contractility in ectodermal cells (Fig. 2D) and transplanted PGCs into the manipulated environment. Interestingly, transplanted PGCs that migrated within the lower-contractility ectodermal tissue formed blebs more frequently (Fig. 2E), without changing the bleb size (Fig. 2F). Conversely, PGCs transplanted into mesodermal tissue in which contractility was increased (Fig. 2G) formed fewer blebs (Fig. 2H) with no change in bleb size (Fig. 2I). These observations suggest that the cortex tension in cells surrounding the PGCs is an important parameter that determines how often blebs form. However, although the cortex tension of cells in the environment influences the frequency of bleb initiation, this parameter does not affect bleb expansion. This suggests that, in addition to cortical tension, other parameters influence blebbing in these settings. Consistent with the results presented above, the migration speed and track straightness were similar for cells migrating within the control and ectodermal environment in which contractility was lowered (Fig. S4).
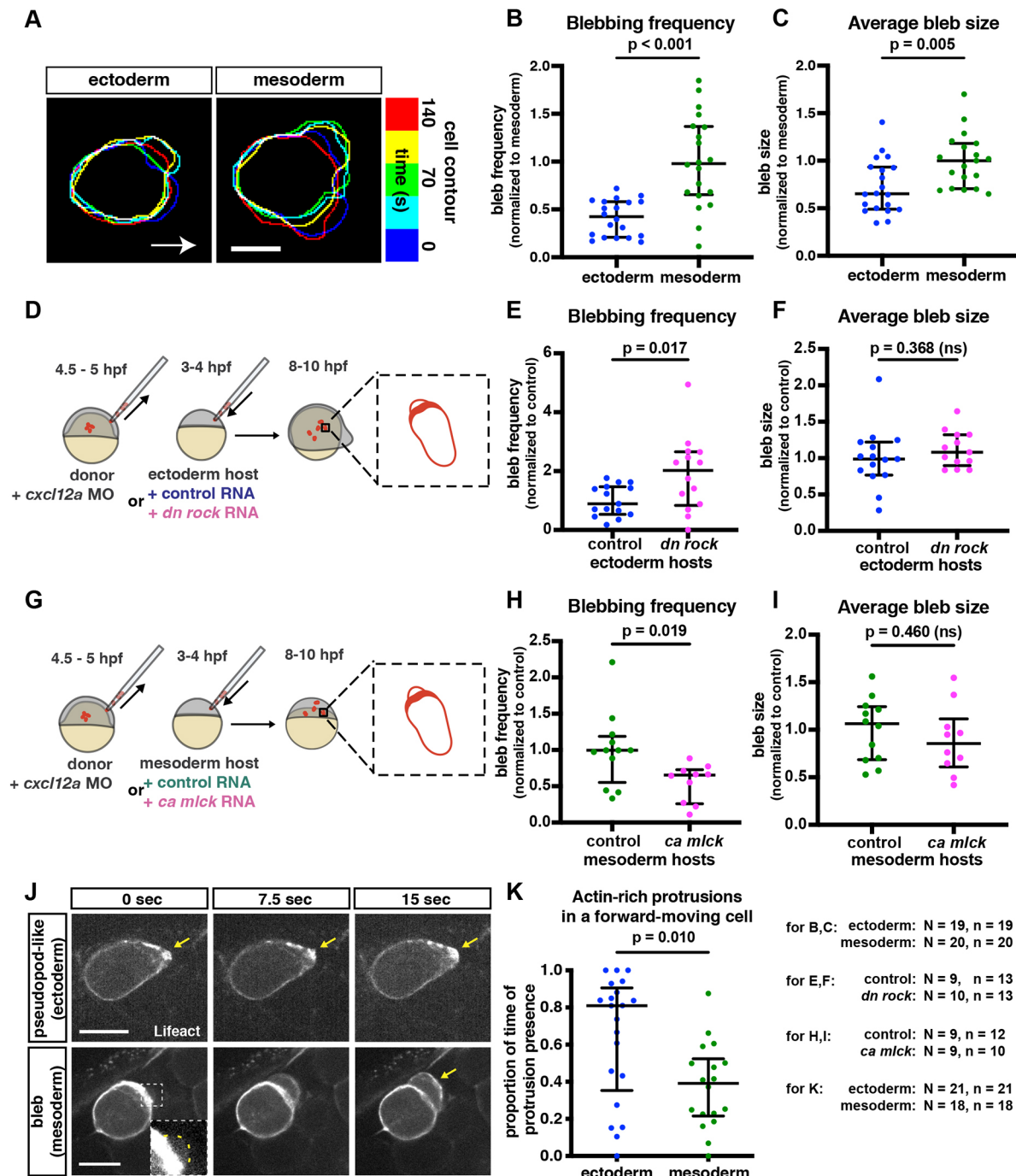
Fig. 2. Alterations in protrusive behavior in PGCs located within different environments. (A) Overlay of cell contours over time of representative PGCs migrating in ectodermal and mesodermal tissues. Contours were aligned to the back of the cell to correct for forward movement. Arrow indicates the direction of migration. Scale bar: 10 µm. (B,C) Blebbing frequency (B) and average bleb size (C) of PGCs moving within converted embryos. For bleb frequency comparison (B), a Mann–Whitney test was performed; for average bleb size (C), a two-tailed *t*-test was performed. (D) The PGC transplantation experiment scheme. Labeled wild-type PGCs were transplanted into ectoderm-converted embryos that were injected at the one-cell stage with either control RNA or a dominant-negative form of ROCK. 4 to 6 h later, blebs formed by the transplanted PGCs were analyzed. (G) A similar transplantation was performed into mesoderm-converted embryos that expressed either control RNA or RNA encoding a constitutively active form of MLCK. (E,F,H,I) Bleb formation frequency (E,H) and average bleb size (F,I) produced by PGCs transplanted into the different environments. Two-tailed *t*-tests were performed. (J) Snapshots of migrating PGCs. Arrows indicate actin enrichment at the edge of protrusion. Inset shows a zoomed-in, contrast-adjusted view of the early-stage bleb, with a yellow dashed line outlining the bleb contour. Scale bars: 15 µm. (K) The proportion of time actin-rich protrusions that are present at the front of a forward-moving cell. Mann–Whitney test was used. The graphs show the median; whiskers indicate the interquartile range (IQR). N and n at the bottom right represent numbers of embryos and cells, respectively.

Alterations in protrusion types

As PGCs mainly extend blebs (Olguin-Olguin et al., 2021), it is surprising that ectoderm-residing cells that generate fewer and smaller blebs migrate similarly to mesoderm-residing PGCs with regard to speed and track straightness (Fig. 1E,F, Fig. S4). To gain further insight into the cellular mechanisms that govern protrusion formation in both cases, we examined the distribution of actin within the protrusions. Interestingly, during active migration phases,

PGCs located within ectodermal tissue formed actin-rich protrusions more often than cells located within mesodermal tissue (Fig. 2J,K). In those cases, actin was continuously present at the constantly advancing leading edge (Movie 1, Fig. 2J, upper panels), in contrast with the temporary lack of actin at the front of the intermittently forming, rapidly expanding bleb (Movie 2, Fig. 2J, lower panels). Interestingly, we found that protrusions characterized by elevated levels of actin at their leading edge form a three-dimensional structure, as do blebs (Movie 3). Based on these characteristics, we conclude that, when located within the ectodermal environment, PGCs adjust their protrusion type and form more actin-driven pseudopod-type protrusions. Importantly, as measured in fibroblasts, an actin cortex-bound membrane exhibits 10 times more tension than blebs that lack actin underneath their membrane (Tinevez et al., 2009). The increased tension in the actin-rich protrusion could make migration more effective within the ectoderm. In the context of the wild-type embryo, this shift could help PGCs exit the ectoderm and reach the developing gonad, which is a mesodermal derivative.

The molecular organization of migrating PGCs in different cellular environments

Next, we examined parameters that could account for the observed alterations in the protrusion types. To this end, we determined the activation state of RhoA and Rac1: Rho-GTPases that control contractility and actin polymerization (Ridley, 2015), and are important for PGC migration (Kardash et al., 2010; Olguin-Olguin et al., 2021). By employing FRET-based sensors, we found that germ cells located within ectodermal tissue exhibited a mild increase in RhoA activity, which was similar at the front and the back of the cell, while Rac1 activity was not altered (Fig. 3A,B, Fig. S5). To examine whether the increase in RhoA activity is associated with an elevation in myosin activity, we employed a myosin light chain (MLC) FRET-based sensor (Yamada et al., 2005) and observed no difference in MLC-FRET between PGCs located in ectoderm or mesoderm (Fig. 3C). Similarly, actin retrograde flow, which is controlled by actin polymerization, adhesion and actomyosin contraction (Renkawitz et al., 2009), did not differ between the two conditions (Fig. 3D,E).

Relevant for this work, in addition to increasing contractility, RhoA activity can promote ezrin, radixin and moesin (ERM) activation (Bagci et al., 2020; Hébert et al., 2008; Matsui et al., 1999), which could inhibit blebbing by linking the membrane to the underlying cortex and endoplasmic reticulum (Charras et al., 2006; Olguin-Olguin et al., 2021). To investigate the possible involvement of ezrin in the altered cell behavior, we examined its distribution around the cell perimeter and found it to be more evenly distributed in PGCs migrating within the ectoderm (Fig. 3F,G). Importantly, a mild increase of RhoA activity in PGCs migrating within the mesoderm resulted in distribution of ezrin that is similar to that observed in ectoderm-residing PGCs (Fig. 3H,I).

The effect of protrusion type change on migration

As presented above, PGC migration speed and track straightness were similar within different environments (Fig. 1E,F, Fig. S4). It is thus possible that protrusion-type shifts reflect adaptations to environment properties, maintaining migration parameters. To test this hypothesis, we examined how increasing the frequency of bleb formation affected PGC migration. To this end, we expressed low levels of a dominant-negative version of Rac1 in PGCs, which led to increased bleb formation (Vidali et al., 2006, Fig. 4A), presumably by reducing the level of actin at the cell cortex. Interestingly, when

migrating within ectodermal environment, such PGCs exhibited a strong reduction in migration speed (47%) and track straightness when compared with control cells (Fig. 4B). This effect was less pronounced in PGCs that were treated in the same way and migrated within mesodermal cells (25%, Fig. 4C). These findings suggest that interfering with the ability of germ cells to adjust their protrusion type in specific environments reduces their migration efficiency.

Plasticity in PGC migration – a model

Based on our results, we present a model that accounts for the alterations in protrusion types we observed in different cellular environments (Fig. 4D). In non-manipulated embryos, PGCs migrate within and in close proximity to the mesoderm, where they more readily form blebs (84% blebs, 16% pseudopods; Olguin-Olguin et al., 2021). In response to interaction with cells that exhibit increased cortical tension (e.g. in ectoderm), PGCs mildly increase their RhoA activity. Such an elevation in RhoA activity in response to an increase in tension in the environment has been described before in other contexts (e.g. Acharya et al., 2018; Gupta et al., 2021). It should be noted that very high levels of RhoA activity lead to stable bleb formation (Liu et al., 2015; Olguin-Olguin et al., 2021; Ruprecht et al., 2015). However, in the context of this work, a moderate elevation of RhoA activity could promote activation of ERM proteins, leading to their broader distribution around the cell perimeter (Bagci et al., 2020). We suggest that, upon interaction with cells with higher cortex tension, PGCs strengthen the attachment of the cortex to the cell membrane, which inhibits blebbing (Charras et al., 2006; Goudarzi et al., 2017; Niggli and Rossy, 2008). Under these circumstances, the cells form more actin-based protrusions.

Previous research has demonstrated that the migration of PGCs is affected by the lack of E-cadherin in the environment (Grimaldi et al., 2020). Specifically, a strong uniform reduction of E-cadherin-based adhesion results in a reduction in migration-track straightness as a result of an increase in retrograde actin flow. Asymmetrical interaction of PGCs with cells devoid of E-cadherin leads to asymmetry in actin retrograde flow such that blebs form away from the manipulated clones, resulting in turning. Cells in ectoderm-converted embryos express lower levels of E-cadherin when compared with that in mesoderm-converted embryos (Krieg et al., 2008), which we could reproduce in our experimental setup (Fig. S6). However, this difference is not as pronounced as that obtained by Grimaldi et al. (Grimaldi et al., 2020), and the retrograde actin flow and migration track straightness are similar in both environments (Fig. 1E,F, Fig. 3E,F). Thus, although E-cadherin function is required for proper migration track straightness (Grimaldi et al., 2020), the differences between the adhesion levels offered by ectodermal and mesodermal cells are not sufficient for affecting this specific parameter.

At this stage, the precise mechanisms by which germ cells sense the cortex tension of cells in their environment are unknown. We have previously characterized interactions of PGCs with the developing gut (Paksa et al., 2016) and the notochord (Gross-Thebing et al., 2020), as well as with cells lacking E-cadherin (Grimaldi et al., 2020). However, the previously described interactions could potentially involve signals that are not purely physical. To examine the cellular response to cues that are purely physical in nature, we introduced dextran-based hydrogels of different stiffnesses into embryos and monitored the interaction of PGCs with the gels. Here, we consider gel stiffness as a parameter related to the cortex tension of cells the PGCs interact with, which
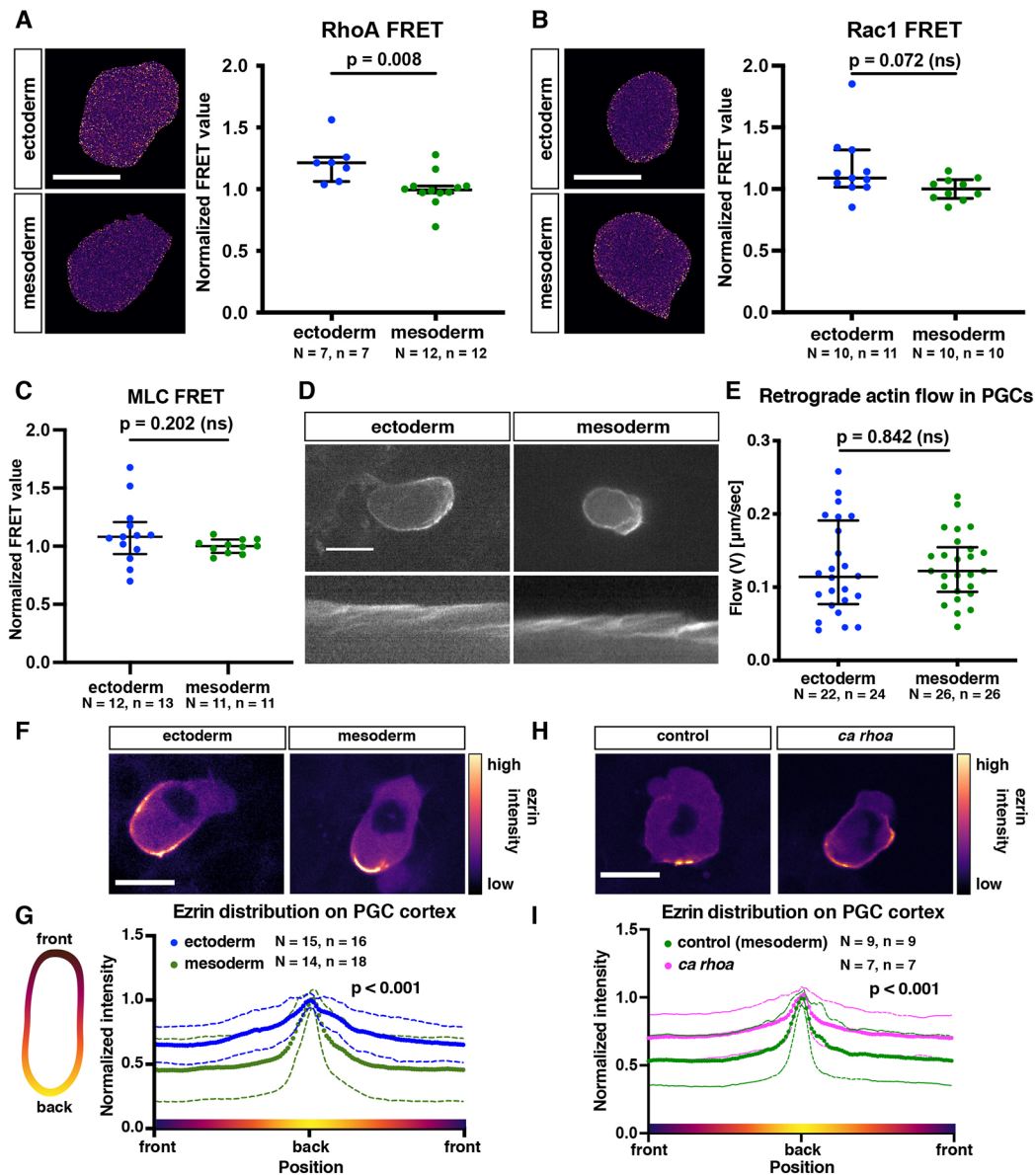
Fig. 3. The role of Rho GTPases in controlling protrusion type formation. (A,B) Normalized whole-cell FRET-based activity measurement of RhoA (A) and Rac1 (B). The graphs show the median; whiskers indicate the interquartile range (IQR). A two-tailed *t*-test was used in A; a Mann-Whitney test was used in B. Scale bars: 15 µm. (C) Normalized whole cell FRET-based myosin light chain phosphorylation levels. The graph shows the median; whiskers indicate the interquartile range (IQR). Two-tailed *t*-test was performed. (D) Representative images of actin flow in PGCs migrating within ectodermal and mesodermal tissues. Kymographs derived from the middle of the cell. Scale bar: 15 µm. (E) Retrograde actin flow speed (V). The graph shows the median; whiskers indicate the interquartile range (IQR). Two tailed *t*-test was performed. (F,H) Representative examples of ezrin-YPet distribution in PGCs residing within converted embryos (F) or in PGCs expressing control RNA or low levels of RNA encoding a constitutively active form of RhoA (H). Scale bars: 15 µm. (G,I) Schematic representation of cortical ezrin distribution around the cell perimeter (left). Cortical ezrin signal was masked and sliced in an angular manner, and the results are presented in the graphs. For each cell, ezrin intensity was normalized to the peak intensity in the cell. Colored dots and solid lines represent the means; dashed lines represent the standard deviations. A Kolmogorov–Smirnov test was performed to compare frequency distributions. *N* and *n* represent numbers of embryos and cells, respectively.

could be perceived in a similar way. In these experiments, we found that cells interacting with stiffer gels exhibited more pronounced changes in actin polarity when compared with their response towards softer gels (Fig. 4E-G, Fig. S7, Movies 4-6). Notably, although both gels are non-adhesive and thus could promote a loss of adhesion-based turning (Grimaldi et al., 2020), they induced very different responses in the migrating cells. Our results therefore suggest that the behavior of PGCs *in vivo* can be affected by physical interactions that are independent of cell-cell adhesion or other specific molecular signals, such as repulsive cues.

Intriguingly, the response of PGCs to the differences in stiffness appears to be associated with actin-rich protrusions. Specifically, 23 out of 27 cases of responses to contact with the gel involved an actin-rich cell front, rather than blebs. These results are consistent with the idea that physical interactions of this type can involve actin-based pushing forces or depend on the proximity of polymerizing actin to the tip of the protrusion (see Gaertner et al., 2022).

We have previously shown that migrating PGCs are extremely robust with respect to their ability to invade and migrate within a wide range of tissues in the developing embryo, allowing all
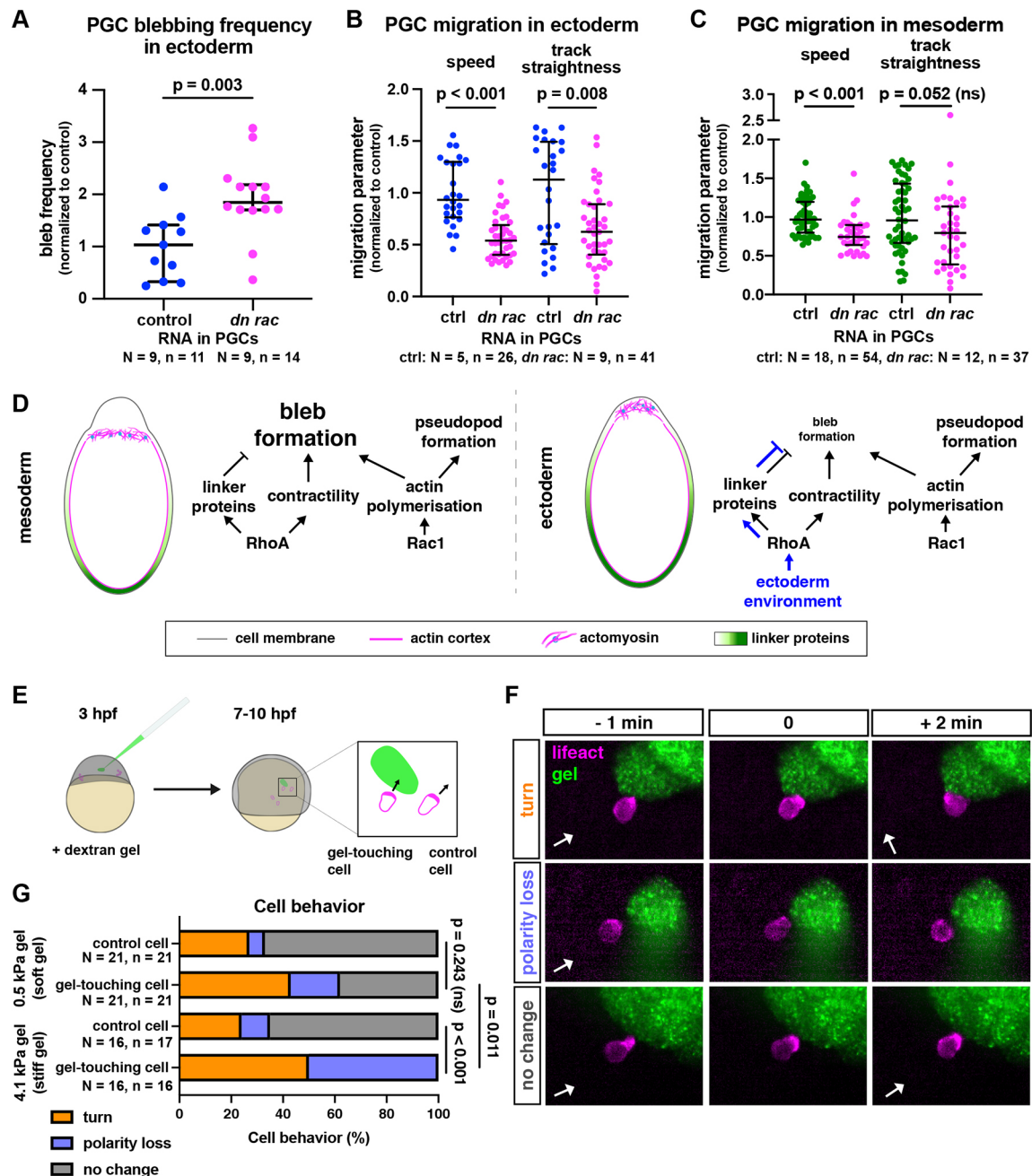
Fig. 4. Effect of blebbing and physical barriers on PGC migration and polarity. (A) Blebbing frequency in PGCs that reside within ectodermal tissues and express control RNA or RNA encoding a dominant-negative version of Rac1. A two-tailed *t*-test was performed. (B,C) Speed and track straightness of PGCs expressing control RNA or a dominant-negative version of Rac1, migrating among converted ectodermal cells (B) or mesodermal cells (C). A Mann–Whitney test was performed for track straightness comparison in B and both comparisons in C, a two-tailed *t*-test was performed for speed comparison in B. The graphs show the median; whiskers indicate the interquartile range (IQR) (D) A model illustrating molecular interactions that lead to the protrusion-type shift in different environments. (E) Illustration of the gel injection experiment. Mutant *cxcr4b*^{−/−} embryos were injected with a dextran gel of 0.5 kPa or 4.1 kPa stiffness at 3 hpf and were imaged 4 h later. As cells migrate non-directionally, some stochastically come in contact with the gel (left cell right-hand box). Alterations in actin distribution were then monitored in cells that came into contact with the gel and in neighboring PGCs that did not encounter the gel (right cell in magnified box). The comparison between the PGCs was performed to control for the inherent periodic loss of polarity observed in PGCs (tumbling; Reichman-Fried et al., 2004). (F) Examples of the reactions of PGCs (lifeact in magenta) to the gel (green). Behaviors were scored based on the change in the polarity of the actin-rich front. The white arrows indicate the direction of the back-front axis of the cell before the interaction with the gel. (G) Quantification of cell behaviors. For statistical tests, Fisher's exact test was performed (comparing the combined turn and loss of polarity behaviors to no change in polarity). A Bonferroni correction for multiple testing was applied. *N* and *n* represent numbers of embryos and cells, respectively.

the PGCs to arrive at their target (Gross-Thebing et al., 2020; Weidinger et al., 1999). Here, we have found that, when located in different environments, PGCs change the types of protrusions they produce, while maintaining their migration speed and track

straightness. This is consistent with our previous observation of an almost even distribution of unguided PGCs across all germ layers (Gross-Thebing et al., 2020). The ability to migrate within tissues of different properties and the associated plasticity have been also

described for leukocytes and cancer cells that change their migration strategies in different *in vitro* settings (e.g. Lämmermann and Germain, 2014; Tozluoğlu et al., 2013). Our findings obtained in an *in vivo* context are thus likely relevant to the migration processes of other cell types that move within tissues with different biophysical properties.

MATERIALS AND METHODS

Zebrafish strains and maintenance

The following zebrafish (*Danio rerio*) lines were used (allele names in parentheses, according to the ZFIN database): wild type (AB), *MZoep*[tz257] (*tdgf1*[tz257/tz257]; Gritsman et al., 1999), *Tg(-1.8gsc:GFP)* (ml1Tg; Doitsidou et al., 2002), *Tg(kop:mCherry-FTASE-UTR-nanos3)* (mu6tg; Tarbashevich et al., 2015), *Tg(kop:EGFP-LIFEACT-UTR-nanos3)* (mu4tg; Hartwig et al., 2014), *Tg(kop:EGFP-FTASE-UTR-nanos3)* (er1Tg; Blaser et al., 2005), *Tg(kop:lifeact-mCherry-utr-nanos3,cryaa:dsred)* (mu118Tg; Grimaldi et al., 2020) and *cxcr4b*[J1049/J1049] (t2603; Knaut et al., 2003). The fish maintenance was supervised by the veterinary office of the city of Muenster, according to the laws of Germany and the state of North Rhine-Westphalia. For details on the fish used in each experiment, see Table S1.

Zebrafish embryo injection

Capped mRNAs were transcribed *in vitro* using the mMessageMachine kit (Invitrogen). A 1 nl drop containing RNAs and/or morpholinos [hereafter (MO), Genetools] was injected into early one-cell stage embryos, unless specified otherwise. The following mRNAs were injected (internal construct designation in parentheses): *lifeact-mCherry-UTR-nanos3* (D554; Olguin-Olguin et al., 2021), *mCherry-FTASE-UTR-nanos3* (A906; Hartwig et al., 2014), *gfp-FTASE-UTR-globin* (393; Boldajipour et al., 2011), *mCherry-FTASE-UTR-globin* (A709; Kardash et al., 2010), *cyclops-UTR-globin* (B836; Sampath et al., 1998), *h2a-tagBFP-SV40polyA* (D846; Compagnon et al., 2014), *RacFRET-UTR-nanos3* (A422; Kardash et al., 2010), *RhoAFRET-UTR-nanos3* (A676; Kardash et al., 2010), *MLCFRET-UTR-nanos3* (A559; Blaser et al., 2006), *tdgf1-UTR-globin* (071; Zhang et al., 1998), *ezrin-YPET-UTR-nanos3* (D025; Olguin-Olguin et al., 2021), *dn-rock-UTR-globin* (E515; this work), *ca-mlck-UTR-globin* (E474; this work), *ca-rhoa-UTR-nanos* (B282; Kardash et al., 2010), *dn-rac-UTR-nos* (482; Olguin-Olguin et al., 2021), *mCherry-h2b-UTR-globin* (B325; Paksa et al., 2016), *vasa-GFP-UTR-vasa* (291; Wolke et al., 2002); *PA-GFP-UTR-globin* or *cd18-UTR-nanos3* were used as control RNA (A918 or 554, respectively; Hartwig et al., 2014). To generate *dn-rock-UTR-globin* construct, zebrafish *rock2* lacking the C-terminus (Marlow et al., 2002) was cloned upstream of *Xenopus globin* 3′UTR. For *ca-mlck-UTR-globin*, a zebrafish *mlck* open reading frame lacking the autoinhibitory domain and the calmodulin binding site (Blaser et al., 2006) was cloned upstream of *Xenopus globin* 3′UTR. Morpholinos used (names used in the ZFIN database are provided in parenthesis) were: *cxcr4b* MO (MO1-cxcr4b), *cxcl12a* MO (MO4-cxcl12a) and *sox32* MO (MO2-sox32). For details on the RNA and morpholinos used in each experiment, see Table S1.

Dextran gel preparation

To introduce artificial physical barriers into live embryos, we injected methacrylated dextran (DexMA) hydrogels. These hydrogels are protein-adsorption resistant, which renders them biologically inert (Trappmann et al., 2017). Owing to their non-swelling nature, the hydrogels retain their initial shape within tissues and are therefore especially suitable for generating barriers *in vivo*. In brief, a solution containing DexMA [71% methacrylation, 4.4% (w/v)], varying amounts of a crosslinker peptide (sequence CGPQGIAGQGC; GenScript) and FluoSpheres 100 nm Yellow Green fluorescent beads (0.01% of gel volume; Invitrogen) in PBS was prepared. The pH was adjusted to 8.0 using 1 M NaOH to initiate hydrogel gelation, and the pre-gel solution was immediately injected into the interstitial space of zebrafish embryos. A final crosslinker concentration of 25.2 mM yielded soft hydrogels (Young's modulus of 0.5±0.1 kPa), whereas stiff hydrogels (Young's modulus of 4.1±0.4 kPa) were produced using 40.4 mM concentration. Importantly, changing the concentration of

crosslinker does not cause a change in the porosity of the gel (Trappmann et al., 2017).

Analysis of PGC response to dextran gels

Embryos were injected at the early one-cell stage, then incubated at 28°C. When the embryos reached 3 hpf, the DexMA gel was injected into the interstitial space. The embryos were then incubated at 25°C. At 7 hpf, the embryos that retained the gel were selected for, dechorionated and imaged using a spinning disc confocal microscope (Visitron Systems) with a 20× magnification water-immersion objective, capturing 100 μm z-stack with 10 μm step size for 1 h at 30 s time intervals. The movies were then analyzed using the Fiji software (Schindelin et al., 2012). To correct for gastrulation tissue movement, the movies were registered based on the imaging channel used for detecting the gel employing the 'Correct 3D drift function'. For the PGCs that came into contact with the gel during the time lapse acquisition, an interval of 6 min was set, starting 1 min before the encounter. In addition, a control cell that did not come into contact with the gel was chosen. Then, based on the change in the front actin polarization during the 6-min interval (1 min before and 5 min after interaction with the gel), the response of both cells was scored. To calculate response time, cells were followed after encountering the gel until turning or polarity loss responses occurred, regardless of the 6-min interval.

Generation of embryos with a single germ layer

For the conversion of embryonic cells into mesodermal tissue, wild-type AB or transgenic females were crossed with *Tg(-1.8gsc:GFP)* males. The embryos were injected at the one-cell stage and kept at 28°C until imaging. Unless mentioned otherwise, 30 min before imaging, the embryos were selected for strong and uniform expression of the GFP signal, dechorionated and prepared for microscopy.

For the conversion of embryonic cells into ectodermal tissue, *MZoep*[tz257] fish that contained the transgenes as indicated in Table S1 were incrossed. The embryos were injected at the one-cell stage, and were then kept at 28°C. Before imaging, the embryos were dechorionated and prepared for microscopy.

Expression of somatic RNAs in PGCs and in cells of the different germ layers

Embryos were fixed at 10 hpf in 4% PFA for 2 h at room temperature. The RNAscope procedure was then performed as described previously (Gross-Thebing et al., 2014). The same probes as those of Gross-Thebing et al. (2020) were used (Biotechne): *sox2* (494861-C3) and *tp63* (475511-C3) to label ectoderm derivatives; *sox17* (494711-C3) to label endodermal cells; and *pcdh8* (494741-C3), *pax8* (494721-C3) and *ntla* (4835511-C2) to label mesodermal cells. The PGCs were imaged on a confocal microscope (Zeiss), using a 40× magnification water-immersion objective, acquiring 24 μm z-stacks with 2 μm step size.

Locating PGCs in converted embryos

Embryos were converted into ectoderm or mesoderm and co-injected with *gfp-FTASE-UTR-globin*, fixed at 8 hpf in 4% PFA for 2 h at room temperature and washed in PBS. Embryos were imaged on a confocal microscope (40× water-immersion objective, 100 μm z-stack with 5 μm step size).

Expression of germline RNA markers in PGCs

Converted and control embryos were fixed at 8 hpf in 4% PFA overnight at 4°C. The RNAscope procedure was then performed as described previously (Gross-Thebing et al., 2014). The following probes (Bio-Techne) were used: *nanos3* (404521-C2) and *vasa* (407271-C3). Embryos were imaged on a confocal microscope using a 63× magnification water-immersion objective, acquiring z-stacks with a 2 μm step size that include the entire PGC (as determined by the *nanos3* probe). The z-stacks were projected with the sum slices method (Fiji), and the average intensity of the *nanos* probe within the cell area was measured (the cell area was determined by the distribution of the *nanos3* probe). Background signal intensity was measured at two locations adjacent to the PGCs,

and the average background intensity was subtracted from the average cell intensity. The same procedure was performed for the *vasa* probe channel.

Tracking of PGCs located within the converted tissues

Embryos were converted into mesoderm or ectoderm as described above. Before imaging, the embryos were ramped in 1% low-melting agarose and imaged between 7 and 8 hpf using a spinning disc confocal microscope (10× water-immersion objective, 250 μm z-stack with 10 μm step size, 1 h with 2-min time interval). PGCs and somatic-cell nuclei (labeled with H2A-tagBFP) were tracked using the Imaris software (Oxford Instruments), where the movement of PGCs relative to that of somatic nuclei was followed.

Analysis of blebbing activity

PGCs were imaged using a spinning disc confocal microscope between 8 and 10 hpf (40× water-immersion objective, 11-min time lapses with 5-s time interval) and cells that were moving forward for longer than 3 min were included in the analysis. To quantify blebbing frequency, blebbing events were counted and divided by the analyzed time period (in minutes). The area of each bleb was measured using the freehand selection tool in Fiji at the time of maximum expansion and this value was divided by the cell area measured at the same time point to provide the 'bleb size' parameter. Blebbing frequency and average bleb size values were normalized to the average value measured in mesoderm conversion.

Analysis of nuclei density

Converted embryos were fixed at 8 hpf in 4% PFA for 2 h at room temperature, washed with PBS and stained with Hoechst (1:10000 in PBS+0.1% Tween, Thermo Fisher Scientific) overnight at 4°C. After washing in PBS, the embryos were ramped in 1% low-melting agarose drop and imaged using confocal microscope (40× objective, z-stacks with 2 μm step size that include the signal from external EVL cells to the yolk). The nuclei were segmented in 3D using the Imaris software and average distance to the five closest neighbors was computed as a measure of cell density.

E-cadherin staining

Converted embryos were fixed at 8 hpf in 4% PFA for 2 h at room temperature, washed with PBS+0.1% Tween and transferred to Dent's solution (20% DMSO and 80% methanol). E-cadherin immunostaining was performed as previously described (Blaser et al., 2006). To detect E-cadherin in zebrafish, mouse polyclonal anti-E-cadherin (610181, BD Biosciences) was used at 1:100 dilution. For labeling, goat anti-mouse secondary antibody conjugated with Alexa Fluor 568 (A-11031, Thermo Fisher Scientific) was used at 1:1000 dilution. Nuclei were stained with Hoechst (1:10000). Embryos were imaged on the confocal microscope, acquiring z-stacks with 2 μm step size. Starting from the layer of EVL cells, 10 consecutive slices were projected using the 'average intensity projection' function in Fiji. The mean intensity of the fixed size area was measured at the center of z-projection. To control for the nonspecific binding of the secondary antibody, control embryos were subjected to the immunostaining procedure without adding the primary antibody. The average intensity value measured in such control embryos was subtracted from the values measured for stained embryos. For each repeat, the values were then normalized to the average value of mesoderm embryos obtained in this repeat.

PGC transplantation

Donor and host embryos were injected (host embryos were 2 h younger). When the donor embryos were about to reach 5 hpf and host embryos 3 hpf, the embryos were dechorionated. PGCs from donor embryos located under the UV fluorescent binocular (Leica) and transplanted using a 50 μm transplantation needle (BioMedical Instruments) into the host embryos. After the transplantation, the host embryos were incubated at 31°C until they reached the 8 hpf stage. Between the 8 and 10 hpf stages, the PGCs that were surrounded by the host cells (marked with mCherry-H2B) were imaged using a spinning disc confocal microscope (40× water-immersion objective, 10 μm z-stack with 5 μm step size, 11 min with 5-s time interval).

The images were subjected to maximum intensity projection and blebbing behavior was analyzed as described above. Individual blebbing frequency and average bleb size values were then normalized to the average value in wild-type host cells (Fig. S2) or control host cells (Fig. 2D,G). In case of transplantations into mesoderm converted embryos (Fig. 2G), host embryos were 0.5 h older than the donor embryos. Before imaging, host embryos were selected for uniform *gsc:GFP* expression.

For tracking (Fig. S4), transplanted embryos were imaged between 8 and 9 hpf using a spinning disc confocal microscope (10× water-immersion objective, 200 μm z-stack with 10 μm step size, 1 h with 2-min time interval). PGCs and somatic cells were then tracked as described above. For each repeat, speed and track straightness of cells were normalized to the average speed and track straightness value of control cells obtained on that experimental day.

FRET measurements

Mesoderm-converted embryos were selected based on their morphology (i.e. cells remaining at the animal pole of the embryos). Between 8 and 10 hpf, the germ cells were imaged using a confocal microscope (40× water-immersion objective, for at least 3 min at 8-s interval) and analyzed as previously described (Tarbashevich et al., 2015). For each repeat, whole-cell FRET values were normalized to the average FRET value of PGCs located within mesodermal tissue obtained on the same day. In addition, in the RhoA FRET experiment, each cell was divided into four sections along the longest axis, with the front and back defined as first and last quarter of the cell. The front/back FRET ratios were then calculated.

Ezrin distribution analysis

Mesoderm-converted embryos were selected based on their morphology. Between 8 and 10 hpf, the germ cells were imaged using a spinning disc confocal microscope (40× water-immersion objective, 10 μm z-stack with 5-μm step size, 11 min with 5-s interval). For each cell, 20 consecutive frames of a polarized, forward-moving cell were selected. Using the Fiji software, the cell cortex was segmented in the following manner: based on lifeact signal, the cell was thresholded and converted into a binary mask. After applying the 'fill holes' function, a copy of the cell mask was subjected to the 'erode' operation four times. Using the 'image-calculator' function, the difference between the original cell mask and the eroded cell mask was generated and used as a cortex mask. Ezrin signal was masked with the cortex mask and analyzed with a custom Python script. The center of the cell was determined as the center of mass of a binarized image of the selected contour. For each image in the stack, the contour was then split in 120 sections of θ=3° wide, and all intensity values within a section were averaged. A Gaussian function of the form

$$I(\theta) = I_0 e^{\frac{-(\theta-\theta_0)^2}{2\sigma^2}} + b$$

was then fitted to the obtained intensity distribution, where σ is the width of the peak in the fluorescence distribution. Finally, for plotting, the data were normalized by the amplitude and shifted so that the peak was centered on 180°.

Actin-rich protrusion time measurements

Embryos were converted into specific germ layers and incubated at 28°C. Between 8 and 10 hpf, the PGCs were imaged using a spinning disc confocal microscope (63× water-immersion objective, 4 min with 500-ms interval). Movies were acquired at a single focal plane that included the front and the back of the cell. We counted the frames that contained the actin-rich front of the forward-moving cell and did not show blebs. We then divided that value by the number of frames in which the cell was polarized and moved forward.

Tracking of PGCs exhibiting increased blebbing

Converted embryos were ramped at 8 hpf in 1% low-melting agarose and imaged on spinning disk confocal microscope (10× water-immersion objective, 200 μm z-stack with 10 μm step size, 1 h with 2-min time interval). PGCs and somatic cells were tracked as described above. For each repeat, speed and track straightness of cells were normalized to the average

speed and track straightness value of respective control cells obtained on that experimental day.

Statistics

All the experiments were repeated at least three times, except for the E-cadherin staining (Fig. S6), which was carried out twice. For each experiment, embryos from the same egg clutch were allocated to a particular treatment group blindly. Investigators were not blinded during the data acquisition or during the analysis, except for the analysis of the hydrogel experiments (Fig. 4E-G and Fig. S7), which was double blinded. Before choosing statistical test, data were tested for normal distribution using D′Agostino-Pearson test. Normally distributed data was subjected to *t*-test, while non-normal distribution was subjected to Mann–Whitney test. In cases where normally distributed data had unequal variances, a *t*-test with Welsch's correction was employed.

Data availability

All relevant data can be found within the article and its supplementary information.

Peer review history

The peer review history is available online at https://journals.biologists.com/dev/lookup/doi/10.1242/dev.200603.reviewer-comments.pdf

References

Acharya, B. R., Nestor-Bergmann, A., Liang, X., Gupta, S., Duszyc, K., Gauquelin, E., Gomez, G. A., Budnar, S., Marcq, P., Jensen, O. E. et al. (2018). A mechanosensitive RhoA pathway that protects epithelia against acute tensile stress. *Dev. Cell* **47**, 439-452.e6. doi:10.1016/j.devcel.2018.09.016

Bagci, H., Sriskandarajah, N., Robert, A., Boulais, J., Elkholi, I. E., Tran, V., Lin, Z.-Y., Thibault, M.-P., Dubé, N., Faubert, D. et al. (2020). Mapping the proximity interaction network of the Rho-family GTPases reveals signalling pathways and regulatory mechanisms. *Nat. Cell Biol.* **22**, 120-134. doi:10.1038/s41556-019-0438-7

Barton, L. J., LeBlanc, M. G. and Lehmann, R. (2016). Finding their way: themes in germ cell migration. *Curr. Opin. Cell Biol.* **42**, 128-137. doi:10.1016/j.ceb.2016.07.007

Blaser, H., Eisenbeiss, S., Neumann, M., Reichman-Fried, M., Thisse, B., Thisse, C. and Raz, E. (2005). Transition from non-motile behaviour to directed migration during early PGC development in zebrafish. *J. Cell Sci.* **118**, 4027-4038. doi:10.1242/jcs.02522

Blaser, H., Reichman-Fried, M., Castanon, I., Dumstrei, K., Marlow, F. L., Kawakami, K., Solnica-Krezel, L., Heisenberg, C.-P. and Raz, E. (2006). Migration of zebrafish primordial germ cells: a role for myosin contraction and cytoplasmic flow. *Dev. Cell* **11**, 613-627. doi:10.1016/j.devcel.2006.09.023

Boldajipour, B., Doitsidou, M., Tarbashevich, K., Laguri, C., Yu, S. R., Ries, J., Dumstrei, K., Thelen, S., Dörries, J., Messerschmidt, E.-M. et al. (2011). Cxcl12 evolution – subfunctionalization of a ligand through altered interaction with the chemokine receptor. *Development* **138**, 2909-2914. doi:10.1242/dev.068379

Charras, G. T., Hu, C.-K., Coughlin, M. and Mitchison, T. J. (2006). Reassembly of contractile actin cortex in cell blebs. *J. Cell Biol.* **175**, 477-490. doi:10.1083/jcb.200602085

Compagnon, J., Barone, V., Rajshekar, S., Kottmeier, R., Pranjic-Ferscha, K., Behrndt, M. and Heisenberg, C.-P. (2014). The notochord breaks bilateral symmetry by controlling cell shapes in the zebrafish laterality organ. *Dev. Cell* **31**, 774-783. doi:10.1016/j.devcel.2014.11.003

Doitsidou, M., Reichman-Fried, M., Stebler, J., Köprunner, M., Dörries, J., Meyer, D., Esguerra, C. V., Leung, T. and Raz, E. (2002). Guidance of primordial germ cell migration by the chemokine SDF-1. *Cell* **111**, 647-659. doi:10.1016/S0092-8674(02)01135-2

Gaertner, F., Reis-Rodrigues, P., de Vries, I., Hons, M., Aguilera, J., Riedl, M., Leithner, A., Tasciyan, S., Kopf, A., Merrin, J. et al. (2022). WASp triggers mechanosensitive actin patches to facilitate immune cell migration in dense tissues. *Dev. Cell* **57**, 47-62.e9. doi:10.1016/j.devcel.2021.11.024

Goudarzi, M., Tarbashevich, K., Mildner, K., Begemann, I., Garcia, J., Paksa, A., Reichman-Fried, M., Mahabaleshwar, H., Blaser, H., Hartwig, J. et al. (2017). Bleb expansion in migrating cells depends on supply of membrane from cell surface invaginations. *Dev. Cell* **43**, 577-587.e5. doi:10.1016/j.devcel.2017.10.030

Grimaldi, C. and Raz, E. (2020). Germ cell migration-Evolutionary issues and current understanding. *Semin. Cell Dev. Biol.* **100**, 152-159. doi:10.1016/j.semcdb.2019.11.015

Grimaldi, C., Schumacher, I., Boquet-Pujadas, A., Tarbashevich, K., Vos, B. E., Bandemer, J., Schick, J., Aalto, A., Olivo-Marin, J.-C., Betz, T. et al. (2020). E-cadherin focuses protrusion formation at the front of migrating cells by impeding actin flow. *Nat. Commun.* **11**, 5397. doi:10.1038/s41467-020-19114-z

Gritsman, K., Zhang, J., Cheng, S., Heckscher, E., Talbot, W. S. and Schier, A. F. (1999). The EGF-CFC Protein One-Eyed Pinhead Is Essential for Nodal Signaling. *Cell* **97**, 121-132. doi:10.1016/S0092-8674(00)80720-5

Gross-Thebing, T., Paksa, A. and Raz, E. (2014). Simultaneous high-resolution detection of multiple transcripts combined with localization of proteins in whole-mount embryos. *BMC Biol.* **12**, 55. doi:10.1186/s12915-014-0055-7

Gross-Thebing, T., Yigit, S., Pfeiffer, J., Reichman-Fried, M., Bandemer, J., Ruckert, C., Rathmer, C., Goudarzi, M., Stehling, M., Tarbashevich, K. et al. (2017). The vertebrate protein dead end maintains primordial germ cell fate by inhibiting somatic differentiation. *Dev. Cell* **43**, 704-715.e5. doi:10.1016/j.devcel.2017.11.019

Gross-Thebing, S., Truszkowski, L., Tenbrinck, D., Sánchez-Iranzo, H., Camelo, C., Westerich, K. J., Singh, A., Maier, P., Prengel, J., Lange, P. et al. (2020). Using migrating cells as probes to illuminate features in live embryonic tissues. *Sci. Adv.* **6**, eabc5546. doi:10.1126/sciadv.abc554

Gupta, S., Duszyc, K., Verma, S., Budnar, S., Liang, X., Gomez, G. A., Marcq, P., Noordstra, I. and Yap, A. S. (2021). Enhanced RhoA signalling stabilizes E-cadherin in migrating epithelial monolayers. *J. Cell Sci.* **134**, jcs258767. doi:10.1242/jcs.258767

Hartwig, J., Tarbashevich, K., Seggewiß, J., Stehling, M., Bandemer, J., Grimaldi, C., Paksa, A., Groß-Thebing, T., Meyen, D. and Raz, E. (2014). Temporal control over the initiation of cell motility by a regulator of G-protein signaling. *Proc. Natl. Acad. Sci.* **111**, 11389-11394. doi:10.1073/pnas.1400043111

Hébert, M., Potin, S., Sebbagh, M., Bertoglio, J., Bréard, J. and Hamelin, J. (2008). Rho-ROCK-Dependent Ezrin-Radixin-Moesin Phosphorylation Regulates Fas-Mediated Apoptosis in Jurkat Cells. *J. Immunol.* **181**, 5963-5973. doi:10.4049/jimmunol.181.9.5963

Kardash, E., Reichman-Fried, M., Maître, J.-L., Boldajipour, B., Papusheva, E., Messerschmidt, E.-M., Heisenberg, C.-P. and Raz, E. (2010). A role for Rho GTPases and cell–cell adhesion in single-cell motility in vivo. *Nat. Cell Biol.* **12**, 47-53. doi:10.1038/ncb2003

Knaut, H., Werz, C., Geisler, R., Nüsslein-Volhard, C., and Tübingen 2000 Screen Consortium. (2003). A zebrafish homologue of the chemokine receptor Cxcr4 is a germ-cell guidance receptor. *Nature* **421**, 279-282. doi:10.1038/nature01338

Krieg, M., Arboleda-Estudillo, Y., Puech, P.-H., Käfer, J., Graner, F., Müller, D. J. and Heisenberg, C.-P. (2008). Tensile forces govern germ-layer organization in zebrafish. *Nat. Cell Biol.* **10**, 429-436. doi:10.1038/ncb1705

Lämmermann, T. and Germain, R. N. (2014). The multiple faces of leukocyte interstitial migration. *Semin. Immunopathol.* **36**, 227-251. doi:10.1007/s00281-014-0418-8

Liu, Y.-J., Le Berre, M., Lautenschlaeger, F., Maiuri, P., Callan-Jones, A., Heuzé, M., Takaki, T., Voituriez, R. and Piel, M. (2015). Confinement and low adhesion induce fast amoeboid migration of slow mesenchymal cells. *Cell* **160**, 659-672. doi:10.1016/j.cell.2015.01.007

Marlow, F., Topczewski, J., Sepich, D. and Solnica-Krezel, L. (2002). Zebrafish Rho kinase 2 acts downstream of Wnt11 to mediate cell polarity and effective convergence and extension movements. *Curr. Biol. CB* **12**, 876-884. doi:10.1016/S0960-9822(02)00864-3

Matsui, T., Yonemura, S., Tsukita, S. and Tsukita, S. (1999). Activation of ERM proteins in vivo by Rho involves phosphatidyl-inositol 4-phosphate 5-kinase

and not ROCK kinases. *Curr. Biol. CB* **9**, 1259-1262. doi:10.1016/S0960-9822(99)80508-9

Niggli, V. and Rossy, J. (2008). Ezrin/radixin/moesin: Versatile controllers of signaling molecules and of the cortical cytoskeleton. *Int. J. Biochem. Cell Biol.* **40**, 344-349. doi:10.1016/j.biocel.2007.02.012

Olguin-Olguin, A., Aalto, A., Maugis, B., Boquet-Pujadas, A., Hoffmann, D., Ermlich, L., Betz, T., Gov, N. S., Reichman-Fried, M. and Raz, E. (2021). Chemokine-biased robust self-organizing polarization of migrating cells in vivo. *Proc. Natl. Acad. Sci.* **118**, e2018480118. doi:10.1073/pnas.2018480118

Paksa, A., Bandemer, J., Hoeckendorf, B., Razin, N., Tarbashevich, K., Minina, S., Meyen, D., Biundo, A., Leidel, S. A., Peyrieras, N. et al. (2016). Repulsive cues combined with physical barriers and cell–cell adhesion determine progenitor cell positioning during organogenesis. *Nat. Commun.* **7**, 11288. doi:10.1038/ncomms11288

Paluch, E. K. and Raz, E. (2013). The role and regulation of blebs in cell migration. *Curr. Opin. Cell Biol.* **25**, 582-590. doi:10.1016/j.ceb.2013.05.005

Reichman-Fried, M., Minina, S. and Raz, E. (2004). Autonomous modes of behavior in primordial germ cell migration. *Dev. Cell* **6**, 589-596. doi:10.1016/S1534-5807(04)00074-7

Renkawitz, J., Schumann, K., Weber, M., Lämmermann, T., Pflicke, H., Piel, M., Polleux, J., Spatz, J. P. and Sixt, M. (2009). Adaptive force transmission in amoeboid cell migration. *Nat. Cell Biol.* **11**, 1438-1443. doi:10.1038/ncb1992

Richardson, B. E. and Lehmann, R. (2010). Mechanisms guiding primordial germ cell migration: strategies from different organisms. *Nat. Rev. Mol. Cell Biol.* **11**, 37-49. doi:10.1038/nrm2815

Ridley, A. J. (2015). Rho GTPase signalling in cell migration. *Curr. Opin. Cell Biol.* **36**, 103-112. doi:10.1016/j.ceb.2015.08.005

Ruprecht, V., Wieser, S., Callan-Jones, A., Smutny, M., Morita, H., Sako, K., Barone, V., Ritsch-Marte, M., Sixt, M., Voituriez, R. et al. (2015). Cortical contractility triggers a stochastic switch to fast amoeboid cell motility. *Cell* **160**, 673-685. doi:10.1016/j.cell.2015.01.008

Sampath, K., Rubinstein, A. L., Cheng, A. M. S., Liang, J. O., Fekany, K., Solnica-Krezel, L., Korzh, V., Halpern, M. E. and Wright, C. V. E. (1998). Induction of the zebrafish ventral brain and floorplate requires cyclops/nodal signalling. *Nature* **395**, 185-189.

Schick, J. and Raz, E. (2022). Blebs—formation, regulation, positioning, and role in amoeboid cell migration. *Front. Cell Dev. Biol.* **10**, 926394. doi:10.3389/fcell.2022.926394

Schindelin, J., Arganda-Carreras, I., Frise, E., Kaynig, V., Longair, M., Pietzsch, T., Preibisch, S., Rueden, C., Saalfeld, S., Schmid, B. et al. (2012). Fiji: an open-source platform for biological-image analysis. *Nat. Methods* **9**, 676-682. doi:10.1038/nmeth.2019

Strome, S. and Updike, D. (2015). Specifying and protecting germ cell fate. *Nat. Rev. Mol. Cell Biol.* **16**, 406-416. doi:10.1038/nrm4009

Talkenberger, K., Cavalcanti-Adam, E. A., Voss-Böhme, A. and Deutsch, A. (2017). Amoeboid-mesenchymal migration plasticity promotes invasion only in complex heterogeneous microenvironments. *Sci. Rep.* **7**, 9237. doi:10.1038/s41598-017-09300-3

Tarbashevich, K., Reichman-Fried, M., Grimaldi, C. and Raz, E. (2015). Chemokine-dependent pH Elevation at the cell front sustains polarity in directionally migrating zebrafish germ cells. *Curr. Biol.* **25**, 1096-1103. doi:10.1016/j.cub.2015.02.071

te Boekhorst, V., Preziosi, L. and Friedl, P. (2016). Plasticity of cell migration in vivo and in silico. *Annu. Rev. Cell Dev. Biol.* **32**, 491-526. doi:10.1146/annurev-cellbio-111315-125201

Tinevez, J.-Y., Schulze, U., Salbreux, G., Roensch, J., Joanny, J.-F. and Paluch, E. (2009). Role of cortical tension in bleb growth. *Proc. Natl. Acad. Sci.* **106**, 18581-18586. doi:10.1073/pnas.0903353106

Tozluoğlu, M., Tournier, A. L., Jenkins, R. P., Hooper, S., Bates, P. A. and Sahai, E. (2013). Matrix geometry determines optimal cancer cell migration strategy and modulates response to interventions. *Nat. Cell Biol.* **15**, 751-762. doi:10.1038/ncb2775

Trappmann, B., Baker, B. M., Polacheck, W. J., Choi, C. K., Burdick, J. A. and Chen, C. S. (2017). Matrix degradability controls multicellularity of 3D cell migration. *Nat. Commun.* **8**, 371. doi:10.1038/s41467-017-00418-6

Vidali, L., Chen, F., Cicchetti, G., Ohta, Y. and Kwiatkowski, D. J. (2006). Rac1-null mouse embryonic fibroblasts are motile and respond to platelet-derived growth factor. *Mol. Biol. Cell* **17**, 2377-2390. doi:10.1091/mbc.e05-10-0955

Weidinger, G., Wolke, U., Koprunner, M., Klinger, M. and Raz, E. (1999). Identification of tissues and patterning events required for distinct steps in early migration of zebrafish primordial germ cells. *Development* **126**, 5295-5307. doi:10.1242/dev.126.23.5295

Wolke, U., Weidinger, G., Köprunner, M. and Raz, E. (2002). Multiple levels of posttranscriptional control lead to germ line-specific gene expression in the Zebrafish. *Curr. Biol.* **12**, 289-294. doi:10.1016/S0960-9822(02)00679-6

Yamada, K. M. and Sixt, M. (2019). Mechanisms of 3D cell migration. *Nat. Rev. Mol. Cell Biol.* **20**, 738-752. doi:10.1038/s41580-019-0172-9

Yamada, A., Hirose, K., Hashimoto, A. and Iino, M. (2005). Real-time imaging of myosin II regulatory light-chain phosphorylation using a new protein biosensor. *Biochem. J.* **385**, 589-594. doi:10.1042/BJ20040778

Zhang, J., Talbot, W. S. and Schier, A. F. (1998). Positional cloning identifies zebrafish one-eyed pinhead as a permissive EGF-related ligand required during gastrulation. *Cell* **92**, 241-251. doi:10.1016/S0092-8674(00)80618-6

DEVELOPMENT
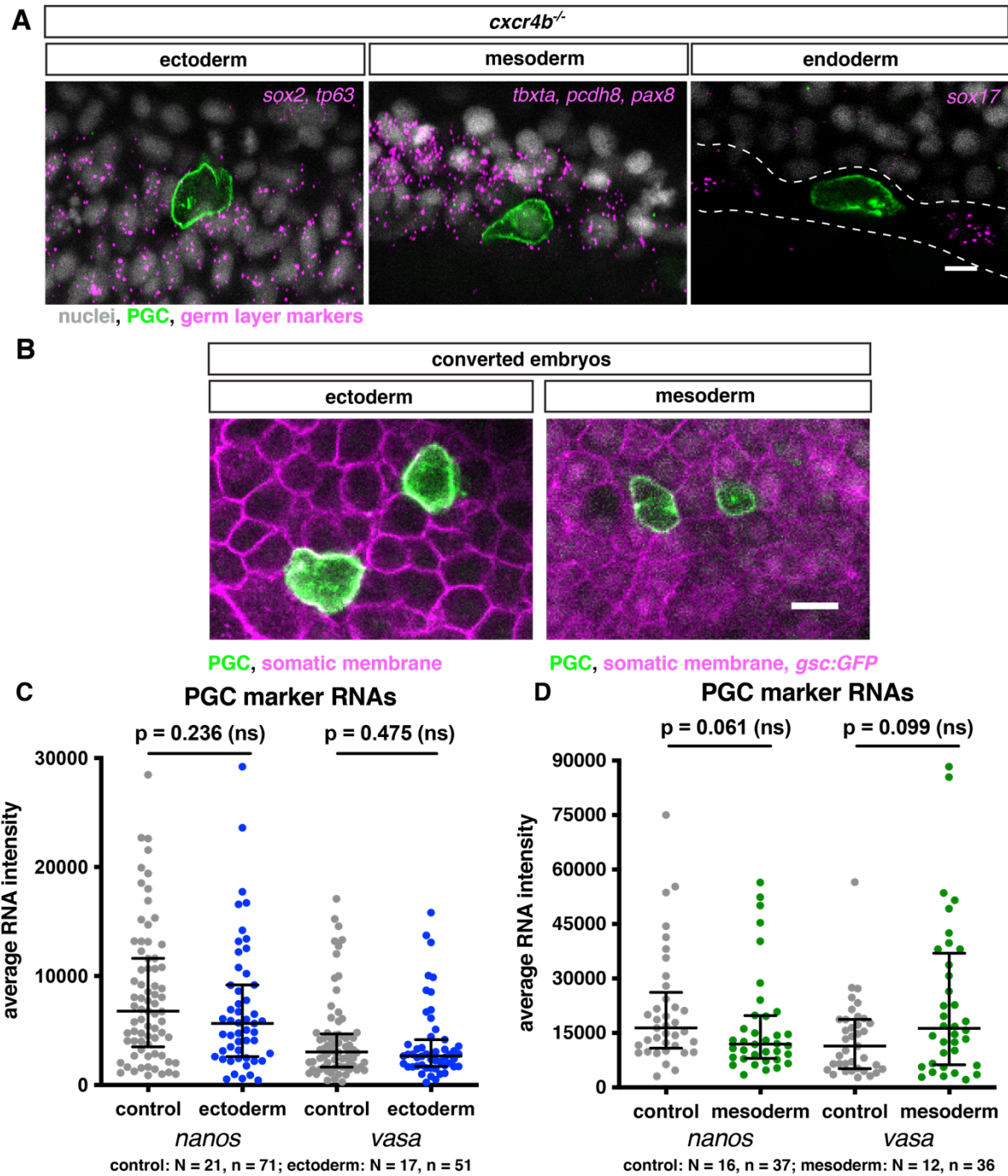
Fig. S1. Preservation of PGC identity in different germ layers. (A), Representative PGCs lacking guidance cues (green) located within tissues of ectodermal, mesodermal and endodermal origin of wild-type embryos (magenta). The thin endodermal layer is marked with a white dashed line. Scale bar, 20 μm. (B) Examples of PGCs (green) residing among the somatic cells of embryos whose cells were converted into ectoderm or mesoderm (left and right panels respectively, magenta). Scale bar, 20 μm. (C-D), Quantification of *nanos* and *vasa* RNA expression levels in PGCs located within control or ectoderm-converted embryos (C) and control or mesoderm-converted embryos (D). The graphs show the median; whiskers indicate the interquartile range (IQR). Mann-Whitney test was performed. N and n represent numbers of embryos and cells, respectively.
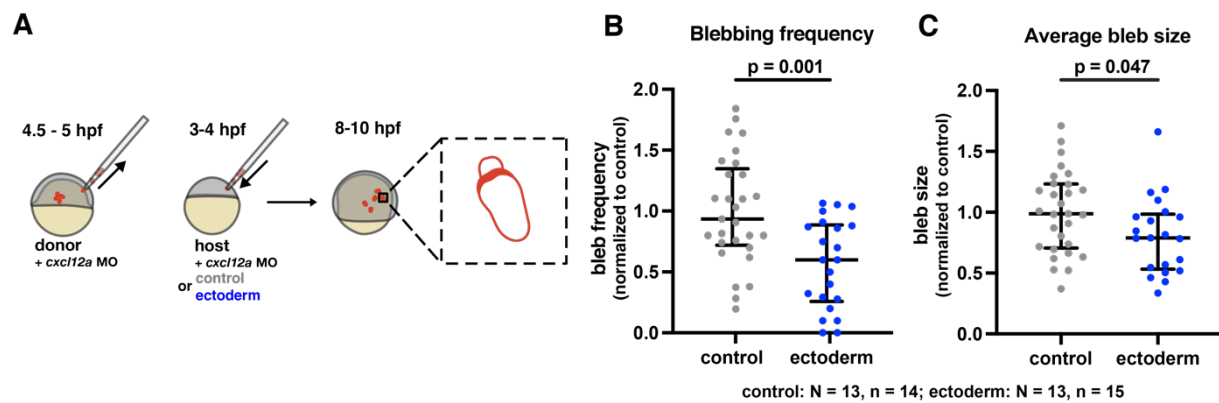
Fig. S2. PGC response to different environments. (A), Illustration of the PGC transplantation experiment. Labeled wild-type PGCs were transplanted into control and ectoderm-converted embryos. After 4 to 6 h, the blebs produced by the transplanted cells were analyzed. Control embryos were wild-type embryos. (B-C), Bleb formation frequency (B) and average bleb size (C) in transplanted PGCs. The graphs show the median; whiskers indicate the interquartile range (IQR). Mann-Whitney test was performed. N and n represent numbers of embryos and cells, respectively.

A

B
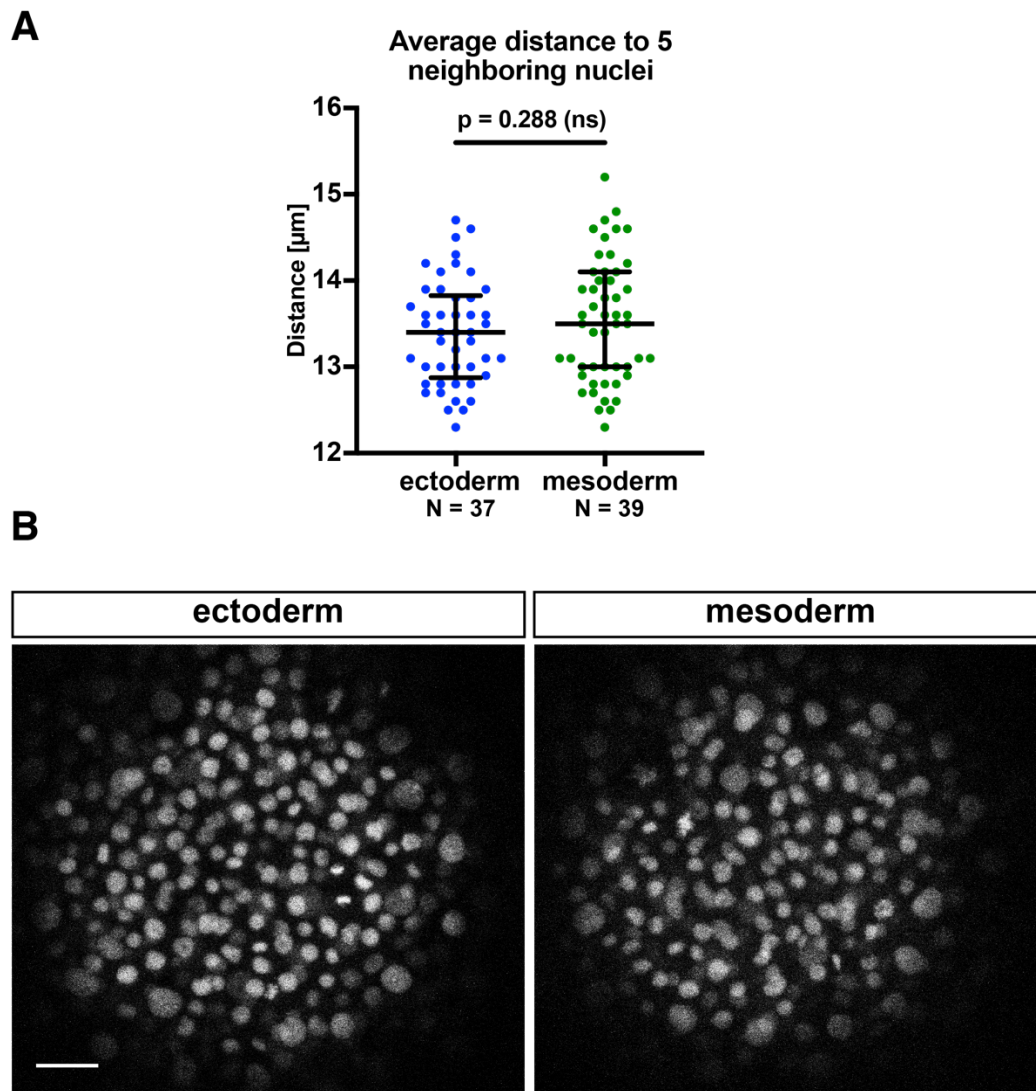
Fig. S3. Cell density in converted embryos. (A) Average distance of somatic cell nuclei to 5 neighboring nuclei in converted ectoderm and mesoderm tissues. The graph shows the median; whiskers indicate the interquartile range (IQR). Ectoderm: Two tailed t-test was performed. N represents number of embryos. (B) Representative images of converted embryos with Hoechst-stained nuclei. Scale bar, 30 µm.

PGC migration - ectoderm
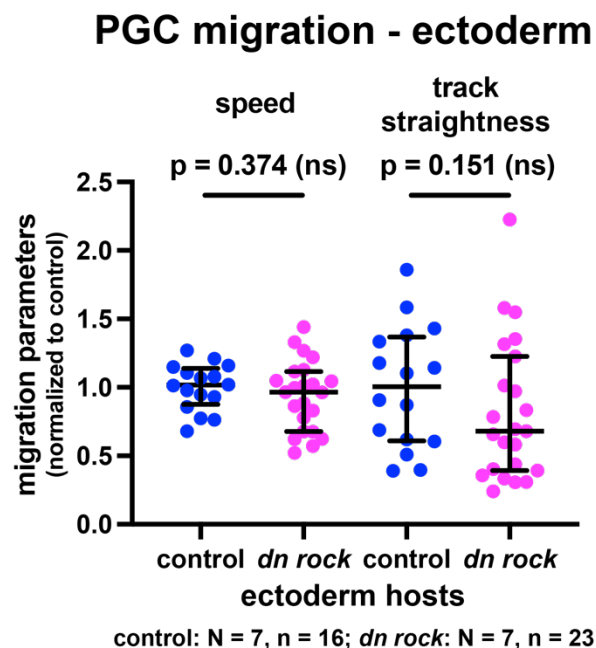
Fig. S4. PGC migration features in modified ectodermal environment. Migration speed and track straightness of PGCs transplanted into ectoderm-converted embryos injected at the 1-cell stage with control RNA or *dn rock* RNA (performed as presented in Fig. 2D). The graph shows the median; whiskers indicate the interquartile range (IQR). Two-tailed t-test was performed for speed comparison, Mann-Whitney test – for track straightness comparison. N and n represent numbers of embryos and cells, respectively.

RhoA activity front/back ratio
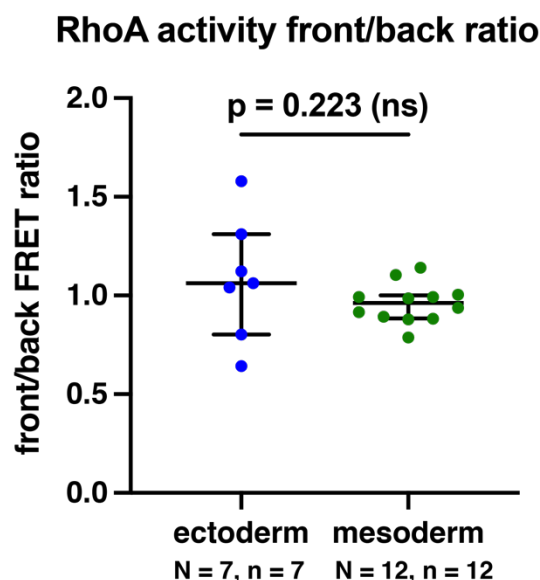
Fig. S5. Distribution of RhoA activity in PGCs migrating within different cellular environments. Ratio between the RhoA FRET levels at the front and the back of the cell. The graph shows the median; whiskers indicate the interquartile range (IQR). Two-tailed t-test was performed. N and n represent numbers of embryos and cells, respectively.

E-cadherin levels

p = 0.003
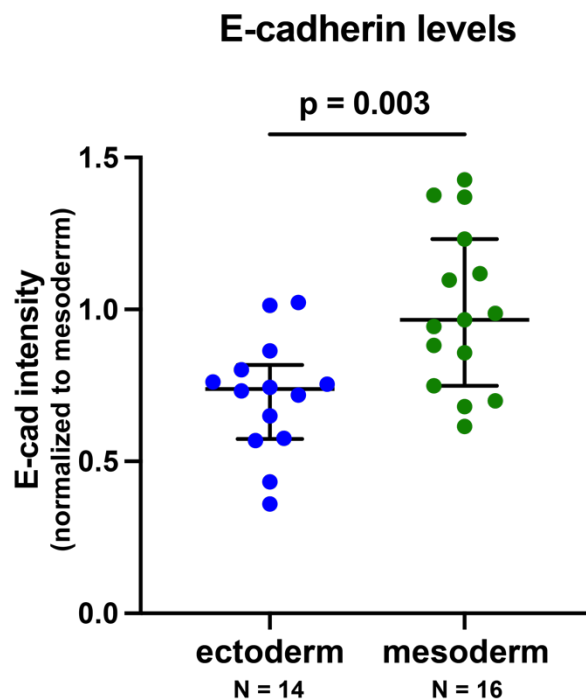
Fig. S6. E-cadherin levels in converted embryos. E-cadherin antibody staining in ectoderm- and mesoderm-converted embryos. The graph shows the median; whiskers indicate the interquartile range (IQR). Two-tailed t-test was performed. N represents number of embryos.

Time required for actin polarity change after contact

p = 0.019
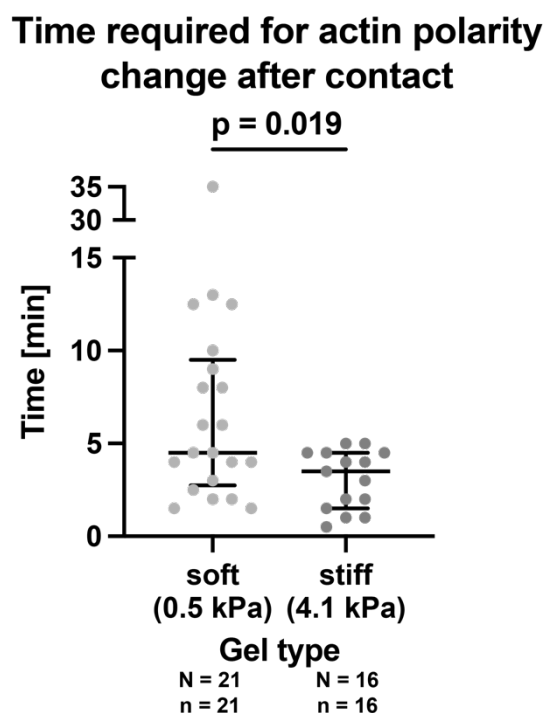
Fig. S7. Time required for a reaction. Plot of the time required for PGCs to change polarity upon contact with the gel, regardless of the interval used in Fig. 4G. The graph shows the median; whiskers indicate the interquartile range (IQR). Mann-Whitney test was performed. N and n represent numbers of embryos and cells, respectively.

**Table S1. Experimental design.**

Click here to download Table S1
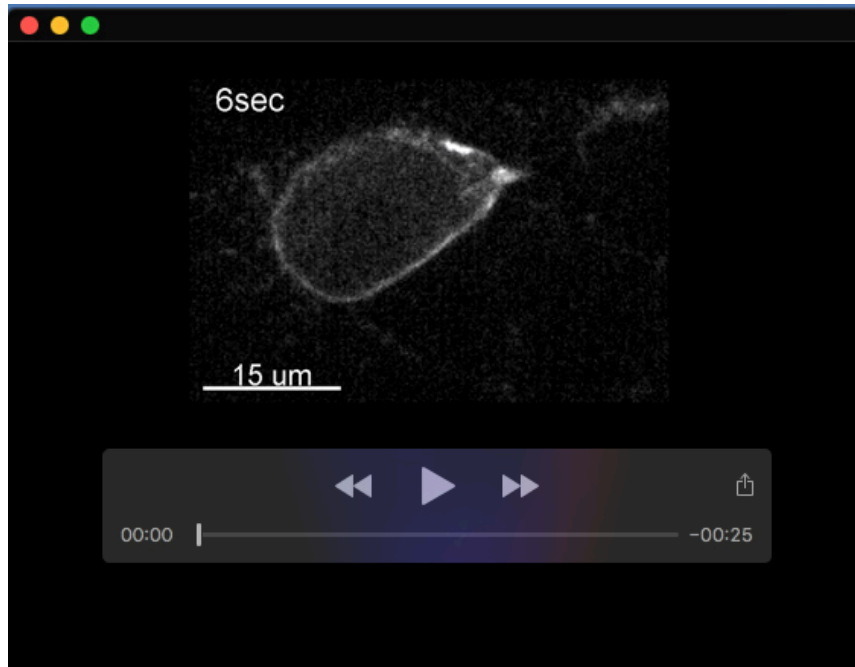
Movie 1. A migrating PGC that generates actin-rich protrusions. Cell was labelled with lifeact-mCherry. Snapshots from the movie are presented in upper panels of Fig 2J.
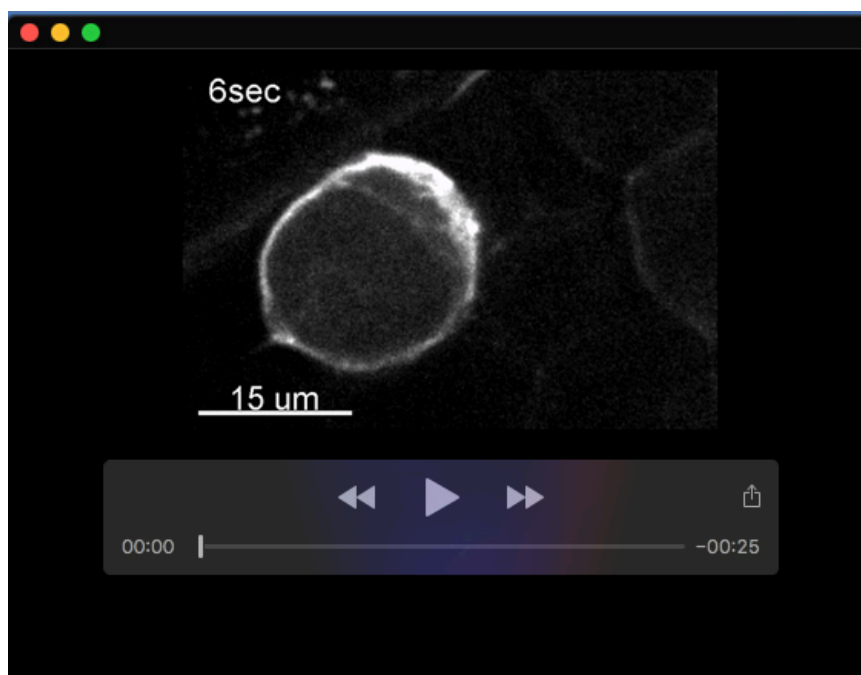

Movie 2. A migrating PGC that generates blebs. Cell was labeled with lifeact-mCherry. Snapshots from the movie are presented in lower panels of Fig 2J.
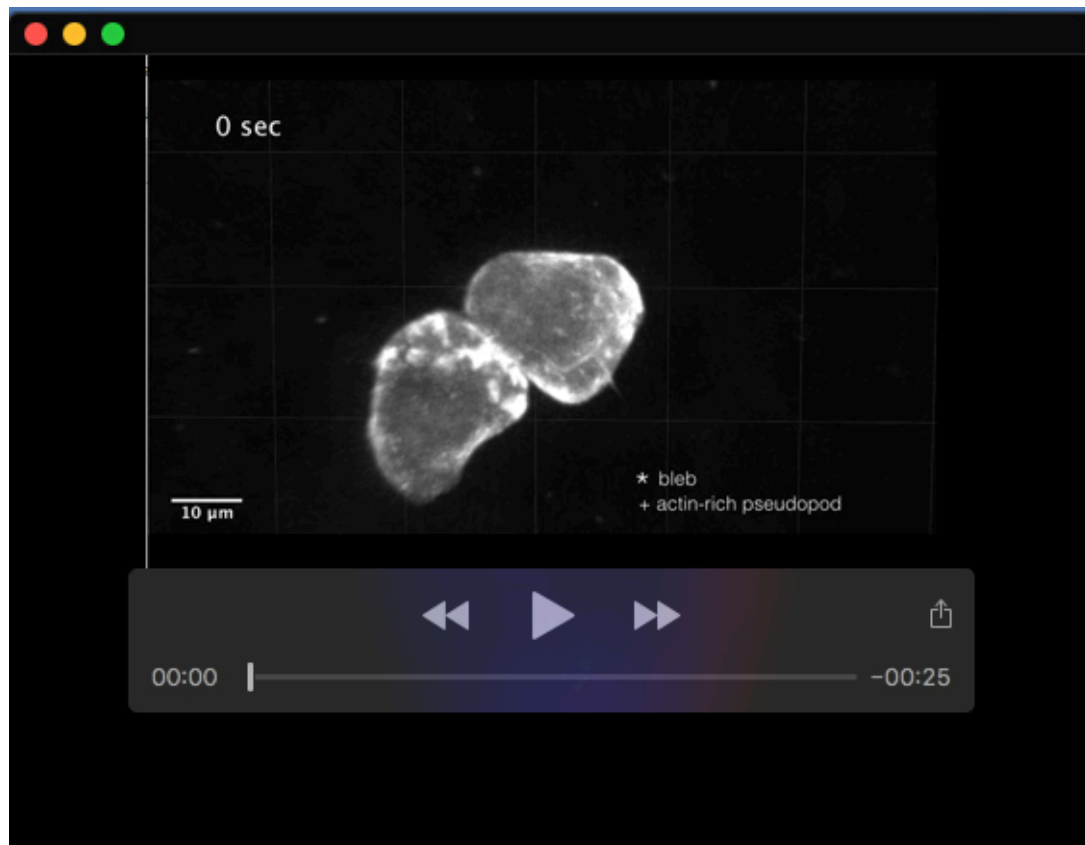
Movie 3. Protrusions in a polarized and an unpolarized cell located within ectodermal environment. 3D projection of Z-stack the includes the whole cell (28 µm stack, with 2µm step size). Cells were labeled with lifeact-mCherry. Top view, a migrating, polarized cell (left), and an apolar cell generating blebs in different directions (right). Side view, with actin enrichments segmented using the "Surfaces" function of Imaris. Actin-rich pseudopods and blebs that are clearly visible in both views are marked with plus (+) and asterisk (*) symbols, respectively. The segmented actin enrichment is always present at the front of pseudopods, in contrast to blebs, in which actin is absent during the initiation and inflation phases. Both types of protrusions are three-dimensional.
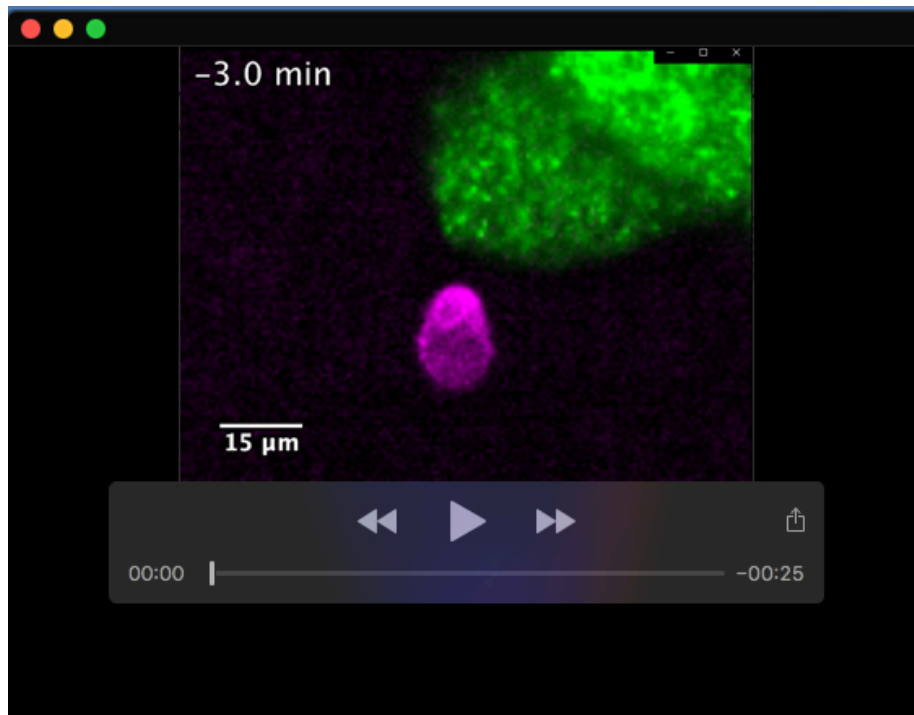
Movie 4. PGC response to contact with the gel. Time 0 shows the estimated moment that the cell (magenta) contacts the gel (green). Snapshots from movies are used in Fig.4F to present a turning response.
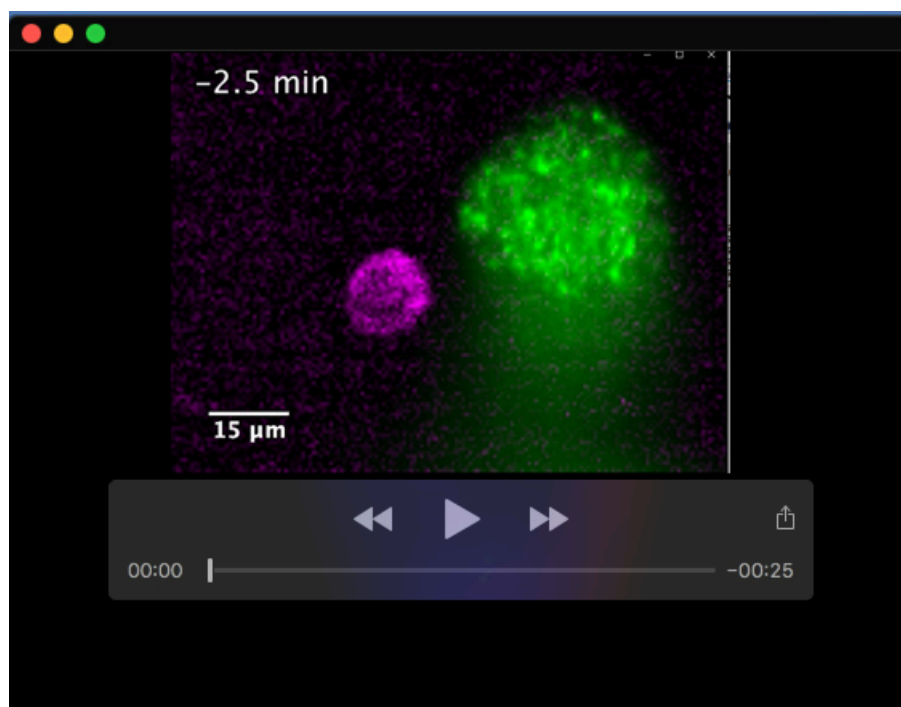
Movie 5. PGC response to contact with the gel. Time 0 shows the estimated moment that the cell (magenta) contacts the gel (green). Snapshots from movies are used in Fig.4F to present loss of polarity.
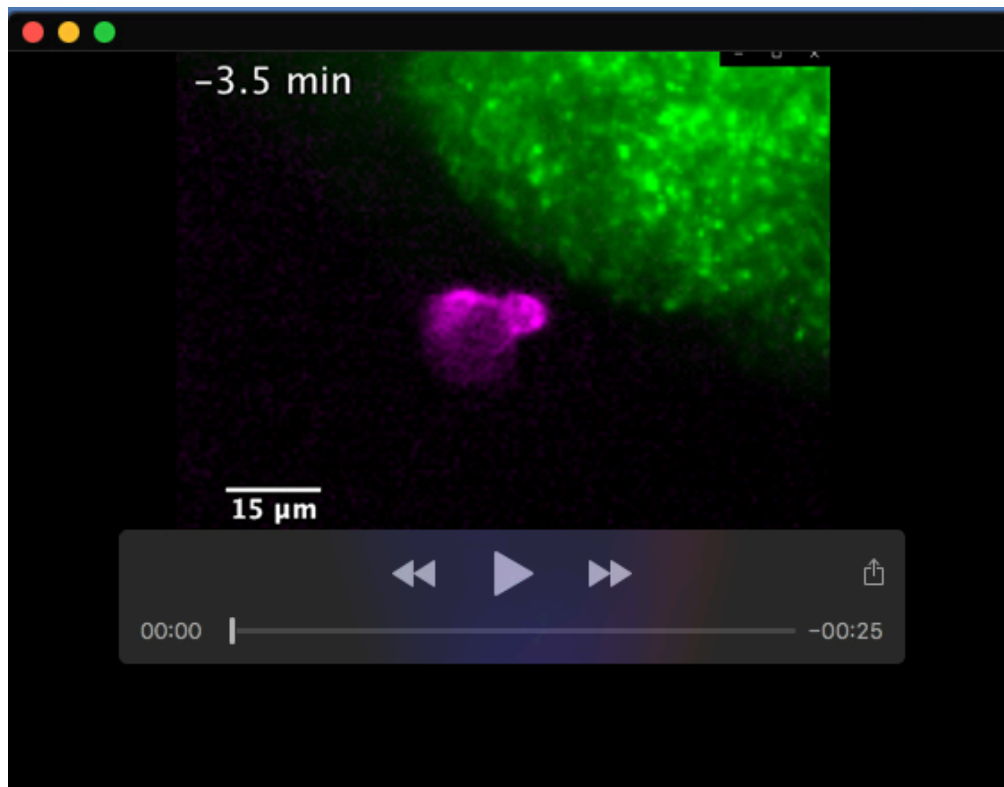
Movie 6. PGC response to contact with the gel. Time 0 shows the estimated moment that the cell (magenta) contacts the gel (green). Snapshots from movies are used in Fig.4F to present no change in polarity.